Materials and Design 97 (2016) 357–363

Contents lists available at ScienceDirect

Materials and Design

journal homepage: www.elsevier.com/locate/matdes

Efficient liquid metallurgy synthesis of Fe–TiB_2 high modulus steels via in-situ reduction of titanium oxides

C. Baron, H. Springer *, D. Raabe

Max-Planck-Institut für Eisenforschung GmbH, 40237 Düsseldorf, Germany

ARTICLE INFO

Article history:
Received 14 December 2015
Received in revised form 16 February 2016
Accepted 18 February 2016
Available online 21 February 2016

Keywords:
Steel
Metal-matrix-composites
Liquid metallurgy
Aluminothermic reduction
Density
Young's modulus

ABSTRACT

We studied the in-situ reduction of Ti oxides by Al as an alternative and cost effective route for the liquid metallurgical synthesis of low density, high stiffness steels (high modulus steels) containing about 10 vol.% TiB_2. TiO_2, $TiO_{1.83}$ and TiO were inserted via iron tubes into Fe–B melts, with Al either premixed with the oxide powders or liquid in the melt. Depending on Ti oxide type and location of the redox partner Al, greatly differing reaction kinetics, slag formation and corresponding microstructures of the high modulus steels were observed. $TiO_{1.83}$ and TiO premixed with Al showed the highest TiB_2 yield in the cast steel and are thus favourable candidates for the cost effective production of high modulus steels. Based on our findings, a novel synthesis process is proposed, based on filling wire injection into a continuous casting process, allowing the utilisation of the additionally formed oxide particles for the further improvement of the property profile of high modulus steels.

1. Introduction

Weight reduction is the key factor to improve the performance of machines and transportation systems and simultaneously increase their energy efficiency. As a consequence, structural materials design mainly aims at increasing the materials' yield (YS) and ultimate tensile strength (UTS), which allows to decrease the parts' load bearing area and hence its volume and thus weight. In case of steels, which represent the most commonly used structural materials, this led to several ultra-high performance alloys for various applications, f. e. hot-stamping steels in the automotive industry (UTS > 1.5 GPa [1]), maraging steels for aerospace application (UTS > 2,5 GPa [2]) and ultra-high strength pearlitic wires used in tires and cords (UTS > 6,3 GPa [3]). Only in the last decade, density (ρ) reduction has been considered as design criterion and lightweight steels have received considerable attention as so-called 3rd generation high strength steels. Primarily aimed for automotive applications, they allow combining high strength (>1 GPa) and ultra high ductility (>60%) with a significant reduction of ρ down to 6.8 g cm^{-3} [4] which is achieved by adding up to 10 wt.% aluminium (Al) to manganese-carbon alloyed steels. However, the reduced ρ also decreases the steels' Young's modulus (*E*) [5], which – depending on the loading conditions – can eliminate the weight saving potential.

A promising pathway to overcome this detrimental relationship between *E* and ρ is the development of so called high modulus steels (HMS). In these iron (Fe)-based metal-matrix-composites (MMC), the property profiles of strong, ductile and tough steel matrices are blended with stiff and low-density ceramic particles [6]. Compared to other matrix materials such as Al, Fe is favourable as it exhibits a similar specific modulus as Al (E/ρ; about 25 GPa g cm^{-3}), offers widely scalable mechanical properties due to its multitude of equilibrium and non-equilibrium phase transformations, and lower production costs [7].

Despite this advantageous property profile, though, HMS have been mainly produced for small components and niche applications [8]. This is because – as with most MMC materials – the particle size, dispersion and bonding with the matrix could only be controlled by expensive ex-situ synthesis procedures such as powder metallurgy or melt injection/stirring synthesis methods [9,10]. Hence, HMS design utilising titanium diboride (TiB_2) has recently received considerable attention, as TiB_2 is not only a very effective compound for such a purpose (specific modulus about 125 GPa g cm^{-3} [11]), but also can be synthesised in-situ from Fe–Ti–B melts in a pseudo-binary eutectic reaction [12]. Following this, HMS with about 10 to 20 vol.% TiB_2 have been successfully produced and identified as potential candidates for the next generation of advanced high strength steels [6]. Currently the main effort lies on improving the mechanical properties of HMS, especially their so far unsatisfactory ductility and toughness, via alloying additions and control of the solidification kinetics [13].

However, with increasing production volume from small-scale powder metallurgy to large-scale liquid metallurgy, the price of alloying elements becomes more important. According to experimentally validated theoretical predictions [14,15] a fraction of at least 15 vol.% TiB_2 (which corresponds to about 7 wt.% of Ti) is needed to achieve a specific modulus of about 35 GPa g cm^{-3}. Instead of using expensive

* Corresponding author.
E-mail address: h.springer@mpie.de (H. Springer).

http://dx.doi.org/10.1016/j.matdes.2016.02.076
0264-1275/

metallic Ti, it thus seems favourable to utilise the possibility to reduce much more cost-effective Ti oxides by suitable elements such as Al [16]. The feasibility of such an in-situ synthesis procedure has been demonstrated by Anal et al. [17], who produced Fe–TiB_2 composites by the aluminothermic reduction of blue dust (mainly Fe_2O_3), titanium dioxide (TiO_2), boron trioxide (B_2O_3) and Al powder in a quasi self-propagating high-temperature synthesis (SHS) setup. The fabricated composites contained comparatively high TiB_2 fractions (about 35 vol.%, as the focus was on wear resistance) and the aluminothermic reduction only took place under oxygen (O) atmospheres [23].

For volume steel production, however, it appears to be more favourable to let such reduction processes of Ti oxides take place within Fe-based melts (prior to the casting, i.e. without O present), into which the reaction partners are injected by filler wires, which is a common procedure in steel production [18]. It can be expected, however, that the kinetics and extent of the reaction – and thus the final composition, microstructure and properties of such produced HMS – strongly depend on the chosen parameters such as the type (thermodynamic stability) and shape (grit size etc.) of the Ti oxide. Furthermore, the formed oxide particles may not only be disregarded and disposed of as slag's, but could be regarded as attractive candidates to implement into the steel and thus further improve the physical properties of novel HMS.

2. Objective

We investigate the reaction kinetics and synthesis products of the in-situ reduction of titanium oxides by Al within Fe–B based melts, with the aim of identifying the optimum synthesis procedure for an alternative, cost effective liquid metallurgical synthesis of Fe–TiB_2 based high modulus steels.

3. Materials and methods

3.1. Synthesis

Synthesis was performed following the consecutive reaction [17]:

$$Fe_{(l)} + B_{(l)} + Al_{(s,l)} + TiO_{x(s)} \rightarrow Fe_{(l)} + B_{(l)} + Ti_{(l)} + Al_2O_{3(s)} \rightarrow Fe_{(s)} + TiB_{2(s)} + Al_2O_{3(s)} \quad (1)$$

As a consequence of the coupled reduction of Ti oxides and oxidation of Al to Al_2O_3, Ti becomes available for the formation of TiB_2 during solidification. Three types of Ti oxides, i.e. TiO_2, TiO and $TiO_{1.83}$ (non-stoichiometric Ti dioxide; a pre-production step of TiO_2), were injected into the Fe–B melts. The oxidising element Al was either premixed with the Ti oxides or molten together with the Fe–B melt, resulting in six Ti oxide/Al combinations. For all experiments the amounts of Fe, B and Ti (within the Ti oxides) were calculated to obtain 10 vol.% TiB_2 after the reaction is complete, i.e. in the cast ingot. Thereto Al was added stoichiometrically to consume all oxygen (O) released from the reduced Ti oxides, resulting in slightly different melt volumes and respective TiB_2 fractions (9.4 vol.% TiB_2 for experiments with TiO_2; 9.5 with $TiO_{1.83}$:, 9.7 with TiO).

Syntheses were performed by melting ~600 g charges of Fe–B and Fe–B–Al, respectively, in sintered Al_2O_3 crucibles in a vacuum induction furnace (16 kW heating power, 10 kHz, 800 mbar argon (Ar) atmosphere). The Ti oxides and pre-mixtures of Ti oxides with Al were inserted as powders (grain size 40 μm–90 μm) in Fe-tubes (internal diameter 17 mm, wall thickness 0.3 mm). The pre-mixtures of Ti oxides with Al (99.7% purity; grain size 32 μm–100 μm) were obtained by ball milling (3 times for 2 min at 400 rpm in a Fritsch pulverisette 7 premium under Ar atmosphere, using 8 stainless steel balls of 10 mm diameter). After insertion of the powder-filled tubes, the melt was held for 5 min and then cast into water cooled copper moulds with an internal diameter of 20 mm.

3.2. Characterisation

Samples for microstructural and chemical analysis were taken from the top of the cast ingot. Metallographic preparation was performed by standard grinding and polishing techniques. Phase identification was performed on non-etched samples, via electron backscatter diffraction analysis (EBSD; OIM software v.7; 0.1 μm step size), by scanning electron microscopy (SEM; Jeol JSM 6500F) and X-ray diffraction (XRD; Philips PW1830, cobald radiation, proportional detector PW1711). For XRD analysis the material was crushed and sieved to a grain size <90 μm. Phase quantification could be not solely conducted by EBSD due to the widely differing morphology, sizes and hardness (inducing surface reliefs and shadowing effects) of the different constituents. Thus only the ferrite was quantified by EBSD, while the TiB_2 fractions were determined by image analysis software (imageJ 1.46r) on SEM micrographs in backscattered electron contrast (BSE) of samples etched in 1% Nital solution. The only remaining phase in the cast ingot Fe_2B was determined by subtracting the fractions of TiB_2 from those of ferrite, respectively. Mass density measurements were performed on machined chippings under protective atmosphere in a gas pycnometer (Micromeritics Accupyc 1330). *E* values were measured by a Grindosonic MK5 "Industrial" excitation system (flexural vibration resonance) on cylindrical specimens (6 mm diameter, 40 mm long).

Residues left in the crucible after melting were analysed by wet chemical analysis and XRD. The residues were removed from the crucible, crushed to coarse powder for chemical analysis and fine powder (sieved to particles <90 μm) for XRD analysis as the cast material.

4. Results

4.1. Reactions during synthesis

Fig. 1 shows a schematic sketch of the general progression of reaction intensity and the temperature change during the casting experiments which were assessed visually. In general, reaction characteristics after tube insertion seemed not to alter greatly, but reaction starting time and intensity varied strongly for the different Ti oxides/Al combinations. After tube-insertion a slight decrease of the melt temperature followed by a minor temperature increase linked to a minor reaction could be observed. This was followed by a moderate delay time (>60 s) with a slight melt temperature increase. The subsequent strong exothermic reaction was connected to a major melt temperature increase. After subsiding reaction the melting temperature decreased slightly.

Experiments with TiO_2 and $TiO_{1.83}$ combined with Al in the melt were typically coupled to formation of strong smoke during reaction.

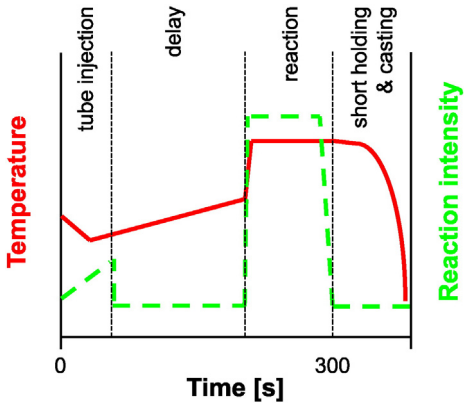

Fig. 1. Schematic illustration of the qualitative development of the reaction intensity and melt temperature for the synthesis of high modulus steels by utilising the aluminothermic reduction of Ti oxides.

Compact low density reaction products quickly floated to the melt surface or got stirred to the crucible walls, leaving only a thin reaction layer on the melt surface. For corresponding experiments with TiO no reaction was visually noticeable. Experiments with premixed Al and Ti-oxides showed slightly stronger reactions, without any formation of smoke. The highest melting temperature was noticed in case of TiO premixed with Al. The low density reaction products appeared to have coarser and less compact appearance than those formed in experiments with pre-molten Al. The reaction procedures do not allow the distinction of a clear trend for the influence of Al location on the reaction kinetics.

4.2. Chemical analysis of the reaction products

The chemical compositions of the cast ingots are plotted in Fig. 2. Experiments performed with Al in the melt are plotted in Fig. 2a, whereas experiments with premixed Al are plotted in Fig. 2b. The calculated nominal composition is represented by the left columns and the actual composition by the right columns. Ti is shown in white, B in light grey, Al in dark grey and O in black. The different Ti/O ratios of the three Ti oxides result in slightly varying Al_2O_3 contents for the pre-calculated ingots. Furthermore it should be noted that the given values in at.% are based on a different mass balance, as the calculated compositions do not consider losses, such as crucible residues as well as vapour and fume losses observed during the experiment.

The actual compositions of the cast ingots for experiments performed with Al in the melt differ substantially from the target values (Fig. 2a). The Ti concentrations decrease from TiO_2 towards TiO, whereas B follows a contrary trend. The corresponding Al concentrations are in case of TiO_2 and $TiO_{1.83}$ roughly around 2.5 at.%, whereas TiO contains with 0.3 at.% Al a much lesser content. The experiments performed with premixed Al (Fig. 2b) show a slightly increasing trend of Ti concentrations from TiO_2 to TiO up to 3.8 at.% and a contrary trend for the B concentrations. The B concentrations of both Al locations are in the same order of magnitude with about 9.0–9.7 at.%, only with TiO and Al in the melt slightly higher values are reached (10.9 at.%). In all cases the corresponding amounts of Ti do not reach the stoichiometric values required to completely consume all B by the formation of TiB_2. Al concentrations measured in the cast ingot do not alter greatly from TiO_2 to TiO, but slightly increase from 0.3 to 0.5 at.%. It is noticeable that the cast ingot Al concentrations in Fig. 2a of TiO_2 (2.0 at.%) and TiO (2.7 at.%) are much higher than those found in all other experiments.

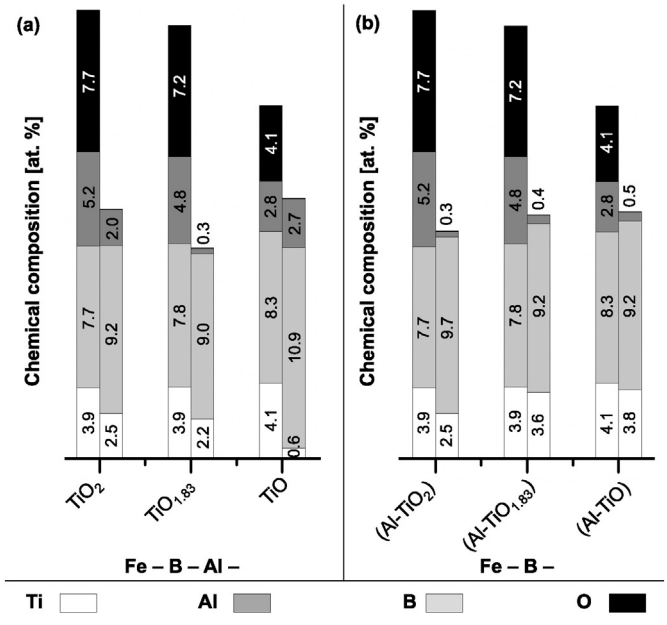

Fig. 2. Chemical composition of the cast ingots (at.%, Fe as balance) for experiments performed with Al in the melt (a) and for Al premixed with the Ti oxides (b). Calculated amounts are shown in the left columns, actual values determined by wet chemical analysis in the right columns, respectively.

For both Al locations (pre-mixed and in the melt) only traces of O (below 0.1 at.%) could be verified in the cast ingots (Fig. 2). In order to clarify the reasons for the absence, analyses of the crucible residues (photographs in Fig. 3) were performed by XRD (Fig. 4). The major constituent is Al_2O_3 (red), accompanied by varying amounts of Ti_2O_3 (green), Fe_2TiO_5 (blue), and small traces of various Fe and Ti compounds (grey). The residues formed in experiments with Al in the melt were compact and sticking to the crucible walls (Fig. 3a, b). The residue for TiO was mainly of metallic nature (Fig. 3c) and no XRD analysis could be performed, as it could not be separated from the Al_2O_3 crucible. Experiments performed with premixed Al led in general to coarser, frothy residues (Fig. 3e, f) and in case of TiO_2 to sintered pillars, which in shape and size resemble the original oxide/Al powder column inserted in the melt. Not considered here and most probably negligible is the possible evaporation of alloying elements during the comparatively long holding times.

4.3. Microstructure of the as-cast ingots

Phase identification is exemplified on a cast ingot sample obtained from the experiment performed with $TiO_{1.83}$ premixed with Al. As can be seen on the colour-coded EBSD phase map with image quality data superimposed in grey scale (Fig. 5), small polygonal particles of TiB_2 (green) and clusters of Fe_2B (blue) are randomly distributed throughout the ferritic Fe (red) matrix. As Fe_2B most probably stems from a ternary eutectic reaction (Liquid → γ Fe + Fe_2B + TiB_2), small amounts of TiB_2 can be found within the networks of Fe_2B. XRD measurements (not shown) confirmed these findings and additionally identified trace amounts of Al_2O_3 and Ti-oxides (below about 2 vol.%).

The different microstructures obtained from the six Ti oxide/Al combinations are shown in direct comparison in the SEM BSE micrographs of Fig. 6. TiB_2 appears in black and Fe_2B in bright grey. Al_2O_3 could not be located by SEM investigations. Microstructures formed at experiments with Al in the melt Fig. 6(a–c) seem to have a decreasing TiB_2 particle content from TiO_2 to TiO. In case of TiO only few small individual TiB_2 particles are found. The morphology of TiB_2 particles varies from hexagonal shape to round or elongated particulates. The particles formed with TiO_2 and $TiO_{1.83}$ are typically bigger (<Ø 5 μm) than those formed with TiO. By contrast, microstructures formed in experiments with premixed Al, as shown in Fig. 6(d–f), seem to have an increasing TiB_2 particle content from TiO_2 to TiO. The TiB_2 particles in Fig. 6d are more angular shaped than the more spiky/plate like TiB_2 morphology observed in Fig. 6e and f. No clear statement about the Fe_2B development can be given due to the strongly deformed matrix and different etching effect.

Phase quantification results of the six experiments are shown in Fig. 7. Calculated amounts of TiB_2 are shown in black squares, measured contents of TiB_2 and Fe_2B in half-filled squares and black triangles, respectively, while the average density values are plotted as empty circles. For experiments performed with Al in the melt (Fig. 7a), the highest TiB_2 content (~3.8 vol.%) was found for the experiment performed with $TiO_{1.83}$. By contrast, the TiB_2 content in the experiments performed with TiO was only ~0.6 vol.%. The Fe_2B phase shows an increasing trend from ~12 vol.% up to ~20 vol.% from TiO_2 to TiO. The highest mass density was found for experiments with $TiO_{1.83}$ (7.63 g cm^{-3}), while experiments using TiO (7.59 g cm^{-3}) and TiO_2 (7.50 g cm^{-3}) are less dense. The TiB_2 content in the cast ingot of experiments performed with premixed Al (Fig. 7b) increases from TiO_2 to TiO (4.5 to 7.5 vol.%). Correspondingly the Fe_2B content decreases from TiO_2 to TiO as well as the mass density. In both Fig. 7a and b the actual TiB_2 content is lower than the target content. The actual TiB_2 contents in Fig. 7a are lower than those in Fig. 7b.

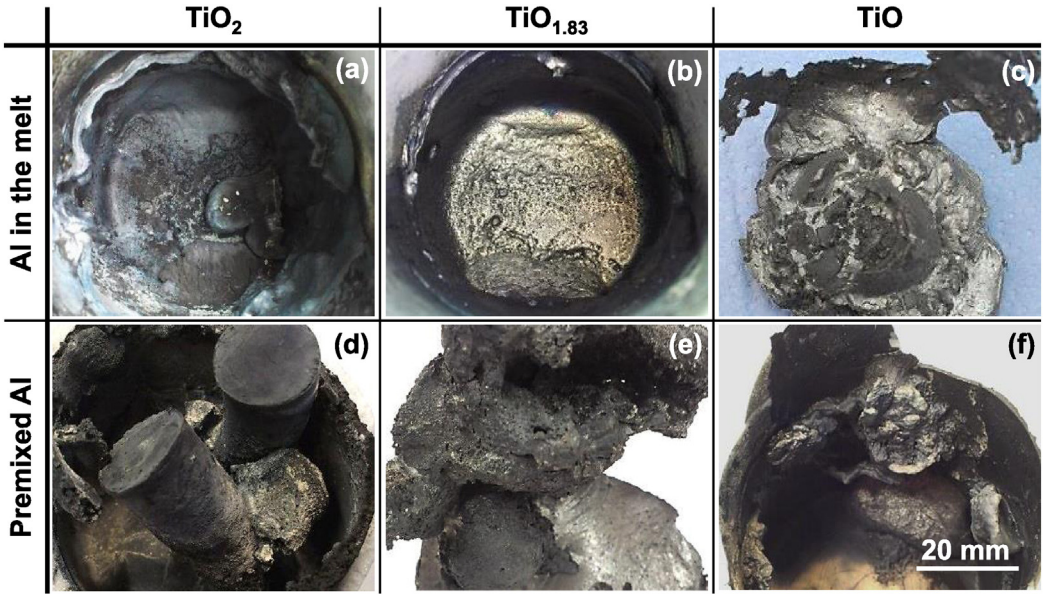

Fig. 3. Photographs of residues left in the crucibles after casting from the different experiments, varying from apparently ceramic content stuck to the crucible walls (a, b), to sintered pillars (d), mostly metallic residue (c) and frothy structures (e, f).

5. Discussion

Fe–TiB_2 based high modulus steels could be successfully produced by utilising the aluminothermic reduction of Ti oxides in Fe–B melts. The observed extent of the TiB_2 formation, however, varied strongly between the six different Ti oxide/Al combinations studied (Figs. 6 and 7). The first of the two consecutive reactions of eq. 1, i.e. the reduction of Ti oxide by the formation of Al_2O_3 (solid in the melt due to its high melting point [19]), can be regarded as the most critical step in the synthesis procedure: once sufficient metallic Ti is available in the melt, the desired compound TiB_2 forms subsequently during solidification [13,20,21]. The standard free energy change, i.e. the thermodynamic driving force, associated with the first reaction step (for 1800 K, based on literature data and equations from [22]) yielded values of about −115 kJ per mol TiO_2 and about −10 kJ per mol TiO, respectively. For $TiO_{1.83}$ no according literature data was available, but as deviations from the stoichiometric composition generally lower the thermodynamic stability of TiO_2 [23], it is reasonable to assume that the respective standard free energy change for reactions with $TiO_{1.83}$ lies between that of values for TiO_2 and TiO. However, the assumption that a higher driving force alone (here $TiO_2 > TiO_{1.83} > TiO$) facilitates the reduction of the Ti oxides, and thus directly translates into higher fractions of TiB_2 in the cast material, holds only vaguely true for experiments in which the Al was present in the melt, while with premixed Al even the opposite trend can be observed (Fig. 7). Incomplete reduction of the Ti oxides can take place as (i) transformation to Ti and O but only of a part of the Ti oxide, and/or (ii) transformation into metastable oxides such as Ti_2O_3 or Fe_2TiO_5 as found in the ceramic residues (Fig. 4). The formation of the latter, though, could also be affected by reactions of the melt with the furnace atmosphere (possible presence of small O quantities in the large VIM furnace) during casting.

Together with the uncertainty of the literature data for the aforementioned calculation of the driving forces, this highlights the relevance of additional factors as e.g. inhibition layers on the injected powders

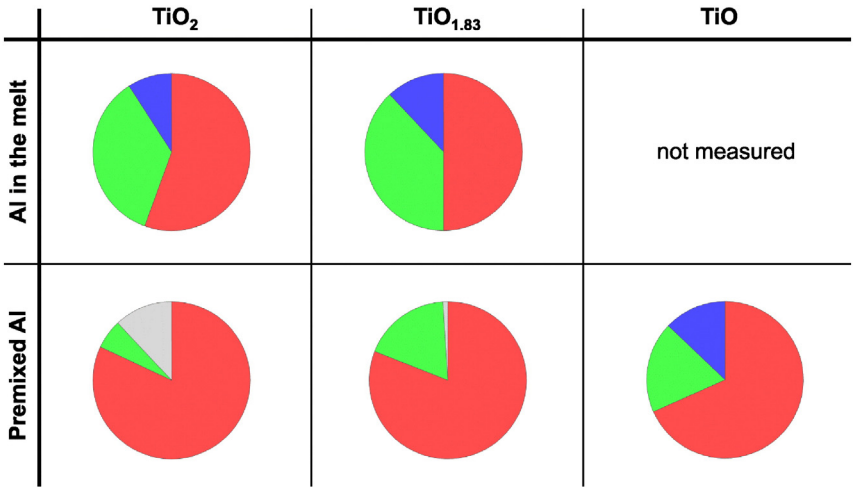

Fig. 4. Colour coded pie charts derived from XRD measurements of the residues in the crucibles after casting from the different experiments. Al_2O_3 is plotted in red, Ti_2O_3 in green, Fe_2TiO_5 in blue and traces of Fe, Fe_2Ti, TiB_2 and FeO are shown in light grey. The mainly metallic residue from experiments performed with TiO and Al in the melt could not be reliably analysed with XRD (strong adhesion to the crucible). (For interpretation of the references to colour in this figure legend, the reader is referred to the web version of this article.)

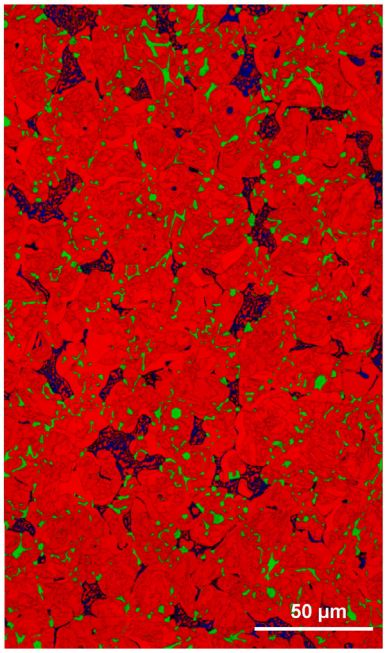

Fig. 5. EBSD phase map with image quality superimposed in grey scale of the cast ingot after inserting $TiO_{1.83}$ premixed with Al into an Fe–B melt, with Fe α in red, TiB_2 in green and the Fe_2B in blue. (For interpretation of the references to colour in this figure legend, the reader is referred to the web version of this article.)

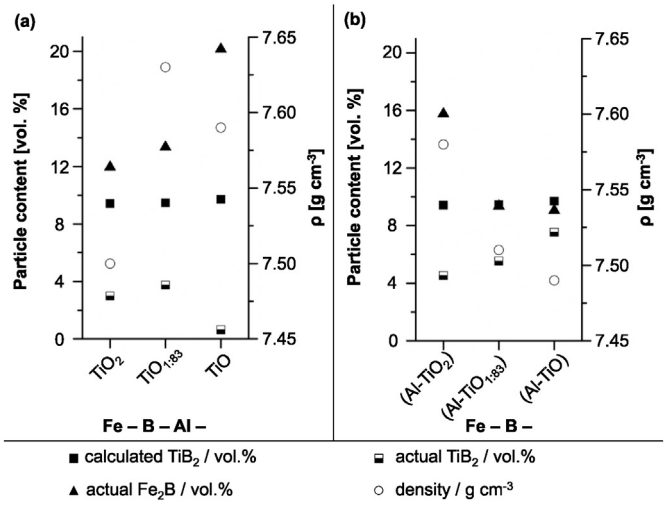

Fig. 7. Overview of the particle contents and density of the cast ingots for experiments performed with Al in the melt (a) and for Al premixed with the Ti oxides (b).

(such as hydride shells around the Ti oxides or pre-oxidation of Al), which can have a significant influence on the activation energy and kinetics of the aluminothermic reaction. The initial cooling effect (before the exothermic aluminothermic reaction begins, Fig. 1) induced by the insertion of the tube could be further minimised by reducing their size down to filler wires (i.e. increasing the ratio between melt/tube volume), as a high melt temperature represents another beneficial factor for the activation energy and reaction kinetics. Another influencing factor which needs to be considered in future experiments is the superheating of the melt as a consequence of the exothermic aluminothermic reaction, as the melt temperature will also alter the cooling rate of the cast ingot and thus its resultant microstructure.

As all these factors are difficult to assess and control, the best setup regarding the type of Ti oxide and location of the Al needs to be carefully optimised for the actual process conditions (e.g. melt temperature, holding times, filler wire thickness, powder grit sizes, milling parameters etc.). In our experimental setup TiO yielded in the highest TiB_2 fraction when premixed with Al, but the lowest one when Al was already present in the melt. TiO_2 and $TiO_{1.83}$, on the other hand, were equally effective irrespective of the Al location. As $TiO_{1.83}$ yielded slightly higher TiB_2 values and is the most cost effective of the used oxide compounds it comes out as the best choice among all studied Ti-oxides when aiming at a robust synthesis of HMS via in-situ reduction processes. The premixing of Al with the Ti oxides is an additional effort, but appears to have a positive effect in general, as respective experiments led to higher TiB_2 fractions (Figs. 6 and 7) and shorter delay times after tube insertion (Fig. 1). However, opposed to experiments with Al in the melt, here the oxides did not form a loose floating slag, but rather an agglomerated, skeleton-like grid (best observed in the case of TiO_2, Fig. 3d), similar to phenomena observed by Sarangi et al. [24]. Such agglomerates – formed as a result of the premixing and compaction of Al powder in the tube – are not only unfavourable as they could get carried into the cast ingot, but also because they can trap TiB_2 in the crucible (Figs. 3 and 4) when hypereutectic Ti(–B) concentrations are reached in the agglomerate and TiB_2 is thus already locally stable in the melt.

As a consequence of these phenomena the targeted TiB_2 concentrations could not be fully reached. Incomplete reduction of the Ti-oxides lowers the Ti content of the melt, and consequently, when most Ti is consumed by the formation of TiB_2, the excess B leads to the formation

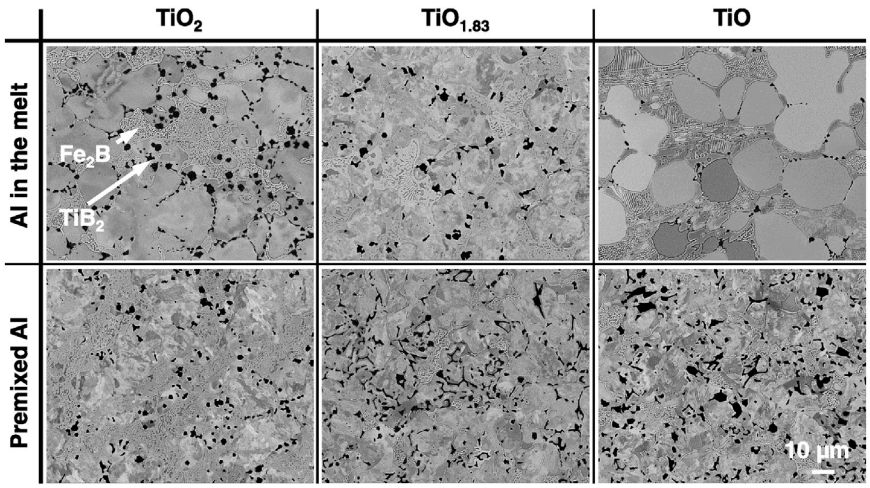

Fig. 6. SEM images (backscatter electron contrast) showing the microstructures of the cast ingots for the different experiments.

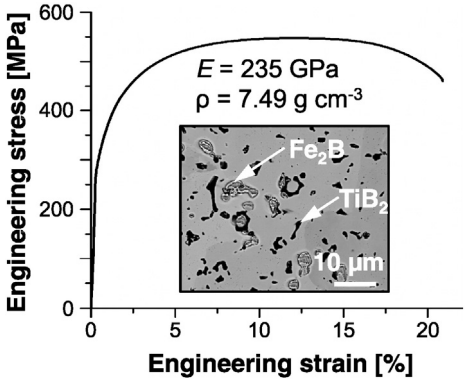

Fig. 8. Engineering stress/strain curve, SEM micrograph and physical properties of a high modulus steel obtained from inserting $TiO_{1.83}$ premixed with Al into an Fe–B melt after additional hot swaging of the cast ingot at 1100 °C.

of Fe_2B according to the Fe–B phase diagram [20,21,25–29] in a ternary eutectic reaction, thus possibly containing traces of TiB_2 [30]. With a specific modulus of about 41 GPa g cm^{-3} [27,31] Fe_2B is not as effective in improving the physical properties of HMS as TiB_2. On the other hand, the Fe_2B networks decorating the grain boundaries of the cast ingot (Figs. 5 and 6) can be spherodized, broken-up, and homogeneously dispersed by thermomechanical processing [21,26,32], improving the mechanical properties. This is demonstrated on a HMS (formed by reduction of TiO premixed with Al) after hot swaging at 1100 °C (Fig. 8), which exhibits a favourable microstructure and thus a striking balance between mechanical (tensile strength and ductility) and physical properties (E and ρ).

The physical properties of HMS could be further improved by the implementation of the formed oxides (specific modulus of Al_2O_3 about 102 GPa g cm^{-3} [27,33,34]). In a conventional discontinuous industrial block casting process though, which our experimental setup resembles, the formed oxides float to the top of the melt after reduction of the Ti oxides in the pan, and were thus removed with the slags before further processing (Fig. 9a). However, if the reduction zone can be placed directly ahead of the solidification front of a continuous casting process, the floatation of the formed oxides may be suppressed (if the velocity of the melt flow and the solidification is high enough) they could thus be incorporated in a HMS (Fig. 9b). The design of such a process is the subject of future work. In order to overcome the difficult wetting of Al_2O_3 by Fe [35–39], other reduction partners for Ti oxides such as yttrium or zirconium could be utilised instead. Additional reduction of B oxides [17] to further reduce production costs is feasible, but as it would greatly increase the amount of oxides, it appears favourable to perform this in an additional step and not in parallel with the reduction of Ti oxides.

6. Summary and conclusions

We studied an alternative and cost-effective route for the liquid metallurgy synthesis of Fe–TiB_2 high modulus steels. By utilising the aluminothermic reduction of Ti oxides instead of alloying costly metallic Ti, stiff and low density steels with about 10 vol.% TiB_2 were produced. TiO_2, $TiO_{1.83}$ and TiO were injected into Fe–B melts. The reduction partner Al was either premixed with the Ti oxide powders or added to the melt prior to the Ti oxide insertion. Reaction kinetics, formation of slags and cast microstructures of the high modulus steels varied greatly depending on the type of Ti oxide type and location of Al. The following conclusions can be drawn:

(1) The TiB_2 content formed in the cast HMS appears to depend mainly on the activation energy and reaction kinetics rather than on the respective driving force of the aluminothermic reduction of the

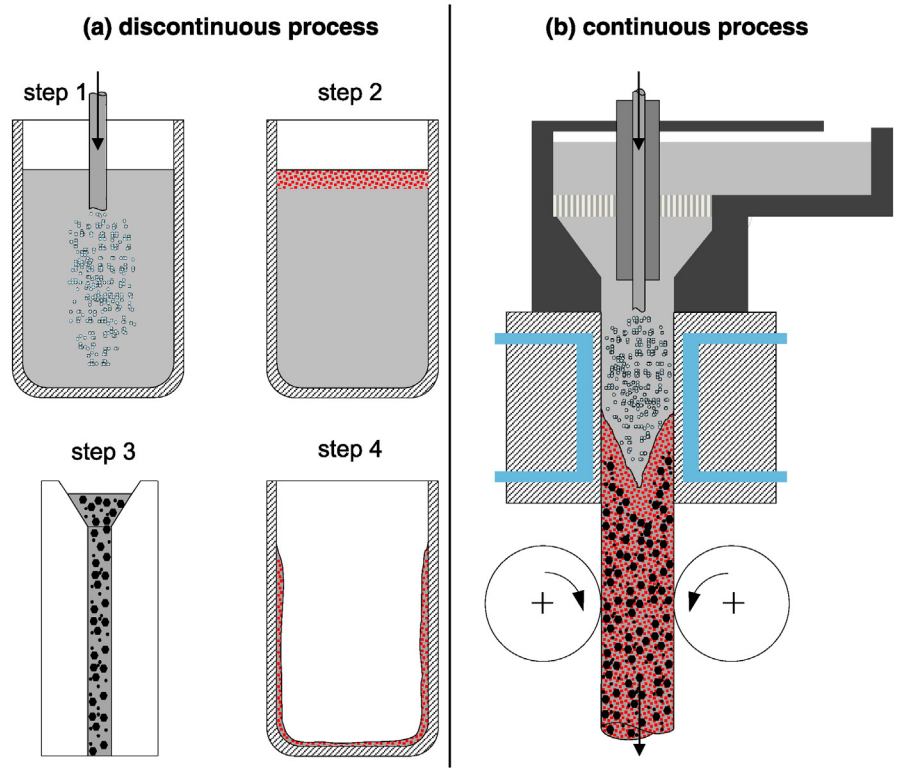

Fig. 9. Schematic sketches of possible synthesis and casting procedures for high modulus steels by utilising the in-situ reduction of Ti oxides: In a discontinuous setup as used for our experiments (a) the (Al-) oxide particles formed after insertion of the Ti oxide (step 1) quickly float to the top of the melt forming a slag (step 2) and after casting (step 3) remain in the crucible (step 4). In a continuous setup (b) the Ti oxides can be inserted directly ahead of the solidification front. Thus the continuous flow of the base melt into the tundish suppresses floatation of the low-density (Al-) oxide particles, ensuring their homogeneous distribution, and making them available for further improving the property profile of high modulus steels.

different Ti oxides. Influencing factors on the latter are, amongst others, the melt temperature, the undercooling induced by tube insertion (and thus by the tube/melt dimensions) and the powder grain size and surface conditions, which need to be carefully adapted and controlled for the respective synthesis process.

(2) The slags formed as a consequence of the aluminothermic reduction consisted mainly of Al_2O_3, together with Ti_2O_3 and traces of Fe, Fe_2Ti, TiB_2 and FeO, with varying fractions depending on the type of Ti oxide and Al location. With Al already present in the melt the slags floated and agglomerated at the crucible walls, while with premixed Al they formed more compact aggregates, which acted as traps for TiB_2.

(3) While premixing Al with the Ti oxides represents and additional processing step, respective experiments consistently yielded larger TiB_2 fractions than those where Al was present in the melt. TiO resulted in the highest TiB_2 content when it was premixed with Al (7.5 vol.%, close to the targeted fraction of 9.7 vol.%), but the lowest (0.6 vol.%) with Al in the melt. Both TiO_2 and $TiO_{1.83}$ showed to be less susceptible to the Al location. In view of the slightly higher TiB_2 values and even lower price$TiO_{1.83}$ can be regarded as the most suitable Ti oxide.

(4) Incomplete reduction of the Ti oxides consequently led to excess B concentration in the melt and thus to the pronounced formation of Fe_2B in the cast HMS. While it is not as effective as TiB_2, it can be evenly dispersed in the HMS matrix via thermomechanical treatments. Hot swaging at 1100 °C of a HMS produced by injecting TiO premixed with Al led to about 550 MPa ultimate tensile strength and 20% ductility, at a density of 7.49 g cm^{-3} and a Young's modulus of 235 GPa.

(5) Only traces of Al_2O_3 were found in the cast HMS due to the floatation and agglomeration of the slags in our discontinuous melting and casting setup. Future work is concerned with utilising such reaction products to improve the property profile of HMS, which requires the development of a continuous casting process with filler wire injection close to the solidification front. For that purpose, other redox partners as Al may be chosen to influence the melt/oxide interaction.

Acknowledgements

M. Kulse and B. Breitbach are acknowledged for their support with synthesis and XRD analysis. Financial support from the Accelerated Metallurgy Project, which is co-funded by the European Commission in the 7th Framework Program (contract NMP4-LA-2011-263206), is gratefully acknowledged.

References

[1] D. Raabe, D. Ponge, O. Dmitrieva, B. Sander, Nanoprecipitate-hardened 1.5 GPa steels with unexpected high ductility, Scr. Mater. 60 (2009) 1141–1144.
[2] P. Würzinger, R. Rabitsch, W. Meyer, Production of maraging steel grades and the influence of specified and nonspecified elements for special applications, J. Mater. Sci. 39 (2004) 7295–7302.
[3] Y.J. Li, P. Choi, S. Goto, C. Borchers, D. Raabe, R. Kirchheim, Evolution of strength and microstructure during annealing of heavily cold-drawn 6.3 GPa hypereutectoid pearlitic steel wire, Acta Mater. 60 (2012) 4005–4016.
[4] Y.-K. Lee, J. Han, Current opinion in medium manganese steel, Mater. Sci. Technol. 31 (2015) 843–856.
[5] W.C. Leslie, Iron and its dilute substitutional solid solutions, Met. Trans. 3 (1972) 5–26.
[6] F. Bonnet, V. Daeschler, G. Petitgand, High modulus steels: new requirement of automotive market. How to take up challenge? Can. Metall. Q. 53 (2014) 243–252.
[7] H. Berns, W. Theisen, Eisenwerkstoffe – Stahl und Gusseisen, Springer, Berlin Heidelberg, 2008.
[8] K. Tanaka, Ultra high modulus steel reinforced with Ti Boride particles, R&D Review of Toyota CRDL, 35 2000, p. 1.
[9] Z. Kulikowski, A. Wisbey, T.M.T. Godfrey, P.S. Goodwin, H.M. Flower, Mechanical properties of high performance lightweight steels, Mater. Sci. Technol. 16 (2000) 925–928.
[10] Z. Kulikowski, T.M.T. Godfrey, A. Wisbey, P.S. Goodwin, F. Langlais, H.M. Flower, et al., Mechanical and microstructural behaviour of a particulate reinforced steel for structural applications, Mater. Sci. Technol. 16 (2000) 1453–1464.
[11] R.G. Munro, Material properties of titanium diboride, J. Res. Nat. Inst. Stand. Technol. 105 (2000) 709–720.
[12] A.K. Shurin, V.E. Panarin, Phase equilibria and structure of Fe–TiB2, Fe–ZrB2 and Fe–HfB2 alloys, J. Res. Nat. Inst. Stand. Technol. 5 (1974) 235–239.
[13] H. Springer, R. Aparicio Fernandez, M.J. Duarte, A. Kostka, D. Raabe, Microstructure refinement for high modulus in-situ metal matrix composite steels via controlled solidification of the system Fe–TiB2, Acta Mater. 96 (2015) 47–56.
[14] Z. Hashin, S. Shtrikman, A variational approach to the theory of the elastic behaviour of multiphase materials, J. Mech. Phys. Solids 11 (1963) 127–140.
[15] K. Tanaka, T. Saito, Phase equilibria in TiB2-reinforced high modulus steel, J. Phase Equilib. 20 (1999) 207–214.
[16] S. Barzilai, M. Aizenshtein, N. Froumin, N. Frage, Mechanism of interface interactions between thermodynamically stable oxides and Al containing melts, Adv. Appl. Ceram. 110 (2011) 15–19.
[17] A. Anal, T.K. Bandyopadhyay, K. Das, Synthesis and characterization of TiB2-reinforced iron-based composites, J. Mater. Process. Technol. 172 (2006) 70–76.
[18] A. Grosse, Entwicklung eines dynamischen Desoxidations- und Legierungsverfahren für die Herstellung aluminiumberuhigter Kohlenstoffstähle beim Bandgießen, Shaker: RWTH Aachen, 2009.
[19] J. Zhang, H.-G. Lee, Numerical modeling of nucleation and growth of inclusions in molten steel based on mean processing parameters, ISIJ Int. 44 (2004) 1629–1638.
[20] F. Bonnet, O. Bouaziz, J.-C. Chevallot, in: A. France (Ed.), Tole d'acier pour la fabrication de structures allegees et procede de fabrication de cette tole 2008, p. 20 (France).
[21] L. He, Y. Liu, J. Li, B. Li, Effects of hot rolling and titanium content on the microstructure and mechanical properties of high boron Fe–B alloys, Mater. Des. 36 (2012) 88–93.
[22] O. Kubaschewski, C.B. Alcock, Metallurgical thermochemistry, 1979.
[23] H. Haerudin, S. Bertel, R. Kramer, Surface stoichiometry of 'titanium suboxide' part I volumetric and FTIR study, J. Chem. Soc. Faraday Trans. 94 (1998) 1481–1487.
[24] A. Sarangi, B. Sarangi, H.S. Ray, S. Misra, Thermoanalytical investigation of the aluminothermic reduction of iron(III) oxide, J. Therm. Anal. 36 (1990) 513–527.
[25] O. Kubaschewski, Iron—binary phase diagrams, Springer, Berlin Heidelberg, 1982.
[26] C. Liu, Z.T. Chen, B.Y. Wang, Q.K. Cai, Microstrture and properties of high boron bearing steel, Acta Metall. Sin. 12 (2002) 248–252.
[27] Y. Feng, Strengthening of steels by ceramic phases, RWTH Aachen, 2013.
[28] C.C. Degnan, P.H. Shipway, The incorporation of self-propagating, high-temperature synthesis-formed Fe–TiB2 into ferrous melts, Metall. Mater. Trans. A 33 (2002) 2973–2983.
[29] C.C. Degnan, P.H. Shipway, A comparison of the reciprocating sliding wear behaviour of steel based metal matrix composites processed from self-propagating high-temperature synthesised Fe–TiC and Fe–TiB2 masteralloys, Wear 252 (2002) 832–841.
[30] A. Antoni-Zdziobek, M. Gospodinova, F. Bonnet, F. Hodaj, Solidification paths in the iron-rich part of the Fe–Ti–B ternary system, J. Alloys Compd. 657 (2016) 302–312.
[31] P. Eckerlin, H. Kandler, Structure data of elements and intermetallic phases, Springer, Berlin Heidelberg, 1971.
[32] R. Choteborsky, M. Kalarikova, Stunova B. Bryksi, The morphology change of iron diboride in the fe–b alloy during deformation, MM Sci. J. 338-40 (2012).
[33] H. Salmang, H. Scholze, Keramik — teil 1: allgemeine grundlagen und wichtige eigenschaften, Springer, 1982.
[34] H. Salmang, H. Scholze, Keramik — teil 2 keramische werkstoffe, Springer, 1983.
[35] M. Humenik, W.D. Kingery, Metal-Ceramic interactions: III, surface tension and wettability of metal–ceramic systems, J. Am. Ceram. Soc. 37 (1954) 18–23.
[36] G.V. Samsonov, The Oxide Handbook, 1973.
[37] Li J-G, Wetting and interfacial bonding of metals with ionocovalent oxides, J. Am. Ceram. Soc. 75 (1992) 3118–3126.
[38] K. Verhiest, S. Mullens, J. Paul, I. De Graeve, N. De Wispelaere, S. Claessens, et al., Experimental study on the contact angle formation of solidified iron–chromium droplets onto yttria ceramic substrates for the yttria/ferrous alloy system with variable chromium content, Ceram. Int. 40 (2014) 2187–2200.
[39] G. Arth, C. Bernhard, A. Samoilov, L. Samek, Entwicklung von stahl-keramik-verbunden mit verminderter dichte, BHM Berg- Huttenmann. Monatsh. 159 (2014) 291–293.